Materials and Design 192 (2020) 108703

Contents lists available at ScienceDirect

Materials and Design

journal homepage: www.elsevier.com/locate/matdes

Influence of Ag alloying on the morphology, structure, mechanical properties, thermal stability and oxidation resistance of multilayered TiSiN/Ti(Ag)N films

A. AL-Rjoub [a,*], A. Cavaleiro [a], F. Fernandes [b]

[a] SEG-CEMMPRE, Department of Mechanical Engineering, University of Coimbra, Rua Luís Reis Santos, 3030-788 Coimbra, Portugal
[b] Department of Control Engineering, Czech Technical University in Prague, Technicka 2, Prague 6 166 27, Czech Republic

HIGHLIGHTS

- Mechanical properties of the TiSiN/Ti(Ag)N films are negatively affected by Ag incorporation
- A multilayered TiSiN/Ti(Ag)N design offers an effective barrier to Ag diffusion.
- Annealing treatment promotes an increase of films crystallinity and hardness.
- Ag incorporation does not affect the onset point of oxidation at high temperatures of the films.
- During oxidation, the presence of Ag in the TiSiN/Ti(Ag)N films gives rise to a less protective Ti-Si-O layer

GRAPHICAL ABSTRACT

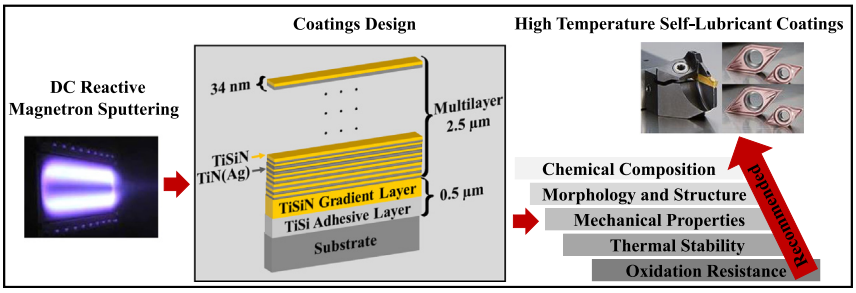

ARTICLE INFO

Article history:
Received 10 January 2020
Received in revised form 27 March 2020
Accepted 28 March 2020
Available online 30 March 2020

Keywords:
TiSiN/Ti(Ag)N films
Structure
Thermal stability
Oxidation resistance

ABSTRACT

Self-lubricant films combine the intrinsic properties of high oxidation resistance coatings with lubricious elements deposited as monolayer and/or multilayered configuration, offering an opportunity to design green coating materials. The present paper reports the influence of Ag additions (range 0–3.2 at.%), considered as low friction material, on the morphology, structure, mechanical properties, thermal stability and oxidation resistance of multilayered TiSiN/TiN(Ag) films deposited by sputtering. The surface morphology of the coatings progressively changed from a well-defined cauliflower structure to a tetrahedral and pyramid-like structure and the cross-section morphology became more compact with Ag incorporation. A decrease of coating's hardness and Young's modulus was observed with Ag additions, due to the incorporation of the soft silver on the structure. The coatings showed excellent thermal stability and revealed a good control to the Ag diffusion towards the surface in protective atmosphere. Ag additions did not affect the onset oxidation point of films. However, the oxidation resistance of the films was reduced with Ag inclusion, due to its additional transportation during the oxidation process, promoting additional paths for ions diffusion, giving rise to a less protective Ti-Si-O layer and contributing to the formation of big crystals of rutile on the top.

1. Introduction

PVD hard coatings for cutting tools is one of the most common efficient solutions used to improve their lifetime in the machining industry. Since the advent of the TiN and CrN films in the 80's, they were widely

* Corresponding author.
E-mail address: abbas.al-rjoub@dem.uc.pt (A. AL-Rjoub).

https://doi.org/10.1016/j.matdes.2020.108703

used as protective materials of the surface of cutting tools working in extreme high temperature, resulting in longer lifetime [1,2]. In the last century, enormous efforts and research works have been devoted to develop new coating systems with better mechanical properties, thermal stability, oxidation and tribological performance. The improvement of the properties of coatings were achieved by different approaches, such as: (i) alloying basic coating systems with a third, fourth or fifth element (e.g. TiSiN [3], TiAlCrN [4], TiAlSiN [5], TiAlBSiN [6]), (ii) developing coatings with multilayer structure (superlattices) or stack layers (e.g. TiN/TiSiN, CrN/TiN [7,8], TiSiN/TiAlN [9,10], TiAlN/CrN [11], AlN/TiN [12], TiAlN/TaAlN [13], TiN-TiCN-TiZrN [14] and titanium/CFRP/aluminium [15], (iii) developing coatings with nanocomposite structure (TiSiN [16], TiAlSiN [17], TiAlCrSiN [18] and VCN-(Ag) [19]) and, (iv) development of self-lubricant films as monolayers or multilayered structure (e.g. TiSiN(Ag) [20], Ti-MoS_2 [21], Ti–Al–V–N [22], TiSi(V)N [23], TiSiN/Ni [24], Ag/AlN [25], Cu/W [26], TiSiN/WS_2 [27], TiSiN/Ag [28] and TiAlNyVN [29]). Self-lubricant coating systems with release of lubricious species have shown an enormous potential to be applied on these components since they are able to increase their performance and to reduce or even eliminate the use of harmful liquid lubrication. However, such a solution does not yet allow to meet the need for high speed machining and green manufacturing required for machining those materials due to: i) their failure at high temperature due to low oxidation resistance and ii) the high temperatures result in strong elements diffusion, leading to the rapid depletion of the lubricious agent and the inoperability of the component (see comprehensive papers in the literature of Voevodin [30], Stone [31] and Aouadi [32]). Thus, the challenge is the adequate control of the lubricant transport to allow low friction and wear over long-term periods. The authors of the current paper in a previous work designed a new self-lubricant coating by combining the nanocomposite structure of TiSiN films (TiN nano-crystallites embedded in a thin amorphous SiNx matrix) alloyed with Ag to fulfil this goal [22,33]. The results showed that the nanocomposite structure of these films worked as an efficient barrier to the Ag diffusion, although, a zone depleted in Ag just some nanometers below the sub-surface of the film could be observed.

Coatings produced as multilayered can offer better mechanical properties than coatings produced as monolayer structure due to the so called superlattice effect [34]. Additionally, the performance of multilayered coatings has been reported to be improved in relation to their corresponding monolayered films for many coating systems [34–36], either due to their better mechanical properties or owing to the crack deflection which often lead to the failure of monolayer coatings [34]. In this work, we produced multilayered TiSiN/Ti(Ag)N films with increasing Ag concentration to evaluate the capacity of the TiSiN layer in the multilayered structure for working as an efficient barrier against the Ag diffusion, with the final goal of observation if the multilayer structure can work as an efficient design for producing coatings with long term lubrication. The diffusion of silver was evaluated by thermal stability tests at protective atmosphere and oxidation resistance tests. Influence of Ag on morphology, structure, mechanical properties of films were also investigated.

2. Experimental

Multilayered TiSiN/TiN(Ag) coatings with increasing Ag concentration were deposited by d.c. reactive magnetron sputtering, working in unbalanced mode, composed by two magnetrons facing each other. Two targets (100 × 200 mm) were used in the depositions: one high purity Ti (99.9%) target, containing 5 mm diameter holes evenly distributed through the preferential erosion zone of the target (race track), and another a high purity composite TiSi (99.9%) target with chemical composition of 88 at.% of Ti and 12 at.% of Si. The amount of Ag on the films was increased by filling the open holes on the Ti target with 0, 4, 8 and 11 Ag pellets, being the remaining holes filled with Ti pellets. A coating with 0 pellets of Ag (i.e. all holes were filled with Ti pellets) was produced for reference purposes. Different types of substrates were used on the depositions: i) polished FeCrAlY alloy substrates (20 × 10 × 1 mm, for thermal annealing tests, hardness and Young's modulus assessment, X-ray diffraction (XRD) and energy dispersive X-ray spectroscopy (EDS chemical composition), ii) Al_2O_3 substrates for thermo-gravimetric analysis (TGA), iii) WC substrates for adhesion critical loads evaluation (scratch tests) and iv) polished ⌀ 25 × 0.5 mm AISI 316 substrates to measure the coatings residual stresses.

Prior placing the substrates in the chamber, they were ultrasonically cleaned in acetone and in alcohol for 15 and 10 min, respectively. The substrates were then mounted in a substrate holder, placed at the center of the chamber, positioned 13 cm from the targets. The chamber was closed and pumped down to a pressure lower than 4×10^{-4} Pa. Before starting the depositions, the substrates were etched for 50 min in an Ar atmosphere by applying a pulsed bias of 500 V and frequency of 250 kHz to the substrate. At the same time the composite TiSi and Ti (Ag) targets were cleaned by applying a power of 800 W to each target, having the shutters in front of them to avoid cross contamination with the substrates. The flow of Ar used for the etching and cleaning process of the targets was 11 sccm which gave a pressure of 0.28 Pa. In order to improve the adhesion of final films the following sequence of interlayer/gradient layers were produced: i) 300 nm TiSi adhesive layer produced from the TiSi composite target applying a power density of 6.5 W/cm^2, Ar flow of 11 sccm, and a pulsed bias −60 V and 250 kHz during 12 min, giving a pressure of 0.30 Pa and ii) a 250 nm gradient TiSiN layer produced keeping the same power as for the interlayer, with increasing N content each minute up to reach the final pressure of 0.35 Pa. After the interlayers, the multilayer structure was grown by applying 6.5 W/cm^2 on Ti(Ag) and TiSi targets, using 11 sccm of Ar and 13 sccm of N (corresponding to a deposition pressure of 0.35 Pa or a partial pressure P_{N2}/P_{Ar} of 0.17) and applying a pulsed bias of −60 V. All the depositions were carried out with the same deposition parameters; the only feature changing was the number of Ag/Ti pellets at the Ti target. The rotation speed of 18 rpm, used for the inter/gradient layers deposition, was decreased down to 0.9 rpm to ensure the production of TiN (Ag) and TiSiN single layers in the multilayer structure with approximately 15 nm and 19 nm in thickness (period of 34 nm), respectively. The deposition time was set as 1 h and 15 min for all of the depositions in order to produce coatings with approximately 3 μm of total thickness, including inter/gradient layers. A summary of the deposition conditions for the growth of the coatings is shown in Table 1. Hereinafter, the coatings will be referenced as Sx, where x represents the silver concentration measured on the multilayered films. Some monolayered films of TiSiN and TiAgN were deposited too, to estimate the Si and Ag concentrations in the individual TiSiN and TiAgN single layers of the multilayer structure as well as to support the XRD diffraction results discussed later. The cross-section/surface morphologies and the thickness of the coatings were studied by scanning electron microscopy (SEM). Chemical composition of films was evaluated by energy dispersive spectroscopy (EDS). Due to the overlapping between the Ti Ll and N Kα X-ray energies in EDS, monolayered TiN and TiSiN films, deposited with increasing Si contents, with the chemical composition measured by electron probe microanalysis (see our previous works [37]), were used as standard for EDS measurements calibration. The measurements were performed on randomly regions of samples surface with an acceleration voltage of 10 keV.

The structure of the films was evaluated in a X'Pert Pro MPD diffractometer with Cu Kα1 radiation (λ = 1.54060 Å, 45 kV and 40 mA) in 2θ range of 20°–80 °C. The XRD diffractograms were either acquired in grazing and conventional diffraction modes.

The adhesion of the films on polished WC substrate was evaluated in a scratch tester equipment by scratching the films with a linearly increasing force from 5 to 70 N, scratch speed of 10 mm/min and loading speed of 100 N/min. The scratch-test apparatus has a spherical Rockwell C indenter of radius of 0.2 mm. The critical loads were determined by optical microscope analysis according to the standard for scratch-test evaluation.

Table 1
Deposition parameters and main properties of the coatings.

Sample	S0	S1	S2	S3
Number of Ag rods	–	4	8	11
TiSi target power density (W/cm^2)	6.5	6.5	6.5	6.5
Ti (Ag) target power density (W/cm^2)	6.5	6.5	6.5	6.5
TiSi target voltage (V)	540–604	589–612	583–607	572–595
Ti(Ag) target voltage (V)	589–598	532–541	531–565	535–563
TiSi target current density (mA/cm^2)	12.0–10.8	11.0–10.6	11.1–10.7	11.4–10.9
Ti(Ag) target current density (mA/cm^2)	11.1–10.9	12.1–12.0	12.2–11.5	12.2–11.6
Rotation speed for TiSi + TiSiN gradient layers (rotation/min) and deposition time	18 24 min	18 24 min	18 24 min	18 24 min
Rotation speed for TiN(Ag) + TiSiN multilayers (rotation/min) deposition time	0.9 1 h:15 min	0.9 1 h:15 min	0.9 1 h:15 min	0.9 1 h:15 min
Residual stress (GPa)	−4.1	−2.7	−2.5	−1.4
Residual stress (GPa) after annealing at 800 °C	−1.9	−1.4	−1.1	−0.1
Hardness (GPa)	26 ± 4	22 ± 4	19 ± 2	18 ± 4
Young's modulus (GPa)	334 ± 28	297 ± 33	293 ± 22	286 ± 23
Elastic strain to failure - H/E	0.078	0.074	0.063	0.062

The hardness and Young's modulus of the samples deposited on FeCrAlY alloy were evaluated by depth-sensing indentation technique (Micro Materials NanoTest) using a Berkovich diamond pyramid indenter, taking into account the indentation depth, which was kept <10% of the coating's thickness, to avoid the effect of the substrate. The tests were performed using applied loads of and 15 mN. 16 measurements were performed for each sample.

The deflection difference between coated and uncoated stainless-steel disks was used to calculate the residual stress of the films using the Stoney equation.

Thermal stability of coatings was evaluated at 800 °C for 2 h in an oven in protective atmosphere (Ar - balance + H_2 - 5 vol%). Then, the surface and cross section morphology of coatings was characterized by SEM, the structure checked by XRD diffraction and the hardness and Young's modulus by nanoindentation.

Thermogravimetric analyses were conducted to the films deposited onto Al_2O_3 substrates to determine the influence of Ag additions on the onset point of oxidation and oxidation resistance of the coatings. To determine the onset point of oxidation, the films were heated from room temperature up to 1200 °C with constant temperature ramp of 20 °C/min, using 50 ml/min of 99.99% purity air. The oxidation weight gain was evaluated at regular 2 s intervals using a micro-balance with an accuracy of 0.01 mg. After determining the onset of oxidation, isothermal oxidation tests were conducted in air atmosphere for 2 h at 800 °C. The oxide phases formed were characterized by XRD diffraction and by SEM analysis; the surface and cross section of the oxidized films were observed.

3. Results and discussion

3.1. Chemical composition

The chemical composition of multilayered TiSiN/TiN(Ag) coatings as measured by EDS is shown in Table 2. As expected, the incorporation of Ag rods to the Ti target leads to the progressive increase of Ag concentration in the films and decrease of the Ti + Si concentration. However, the progressive decrease of the (Ti + Si)/N ratio suggests that over-stoichiometric films are being produced when Ag is added to the films. As the partial pressure P_{Ar}/P_{N2} and total pressure are the same in all the depositions, the increase of N concentration in the films can be, likely, attributed to the replacement of Ti by Ag pellets at the drilled Ti target. As Ag has no affinity for nitrogen, when Ti pellets are replaced by Ag ones, less Ti area is available, being expected an increase of the targets poisoning. Therefore, an excess of N is possible in the film as well as a decrease of the sputtering rate with the consequent decrease of the deposition rate as it will be discussed later. Although maximum Ag content measured in the films was 3.2 at.%, in the individual Ti(Ag)N layers of the multilayer structure the content is slightly higher than the double of that value. Global Si content in the multilayer film was kept in the range of 4.3–4.8 at.% corresponding to a double Si percentage in the TiSiN individual layers of the multilayer structure.

Table 2
Chemical composition of the coatings measured by EDS.

Sample	N at.%	Ti at.%	Si at.%	Ag at.%	(Ti + Si)/N
S0	49.3	46.1	4.6	0	1.03
S1	49.4	45.1	4.6	0.9	1.01
S2	49.9	43.9	4.8	1.4	0.98
S3	50.2	42.3	4.3	3.2	0.93

3.2. Morphology and structure of the coatings

Cross section and surface morphology of multilayered coatings with increasing Ag content is depicted in Fig. 1. Coatings displayed a multilayer structure with columnar growth extending from substrate up to the top surface of the film. The period thickness of the coatings is around 34 nm, independently of the Ag content. Increasing the Ag content, progressively densifies the cross section morphology of the TiN(Ag)/TiSiN multilayered films, in good agreement with the considerable reducing of the globular top surface features. S0 reference film shows a well-defined cauliflower type surface morphology with grains aggregation to form flat larger structures. As the Ag content increased up to 1.4 at.% (Fig. 1k), the size of these flat structures shrinks and smaller crystallites are formed with granular surface morphology. However, the coating with 3.2 at.% of Ag exhibits a tetrahedral and pyramid-like structure which, according to the work of Zhang et al., suggests larger gaps between neighboring TiN pyramids [38]. Although an increase of the deposition rate would be expected with the incorporation of Ag pellets at the Ti target, due to the high sputtering rate of silver as compared to Ti, an opposite trend was observed. This behavior can be explained, as above described, by the higher target poisoning due to the replacement of Ti by Ag pellets. Besides the higher N content in the films, as shown by the (Ti + Si)/N ratio in Table 2, a decrease of the sputtering rate of the poisoned layer is expected. Therefore, in spite of the much higher sputtering rate of Ag pellets, this factor is not enough to counteract the decrease of the fluxes of sputtered Ti and N species from the target with the consequent global decrease of the deposition rate.

The XRD diffractograms of as-deposited multilayered TiSiN/TiN(Ag) coatings acquired in conventional mode are shown in Fig. 2 a) to d). The XRD diffractogram of a monolayered TiAgN film deposited from the Ti target with high number of Ag pellets is also plotted (spectrum e)). All multilayered coatings exhibit a face-centered cubic structure (f.c.c. NaCl type TiN phase ICDD card no. 01-087-0633) with a (111) preferred

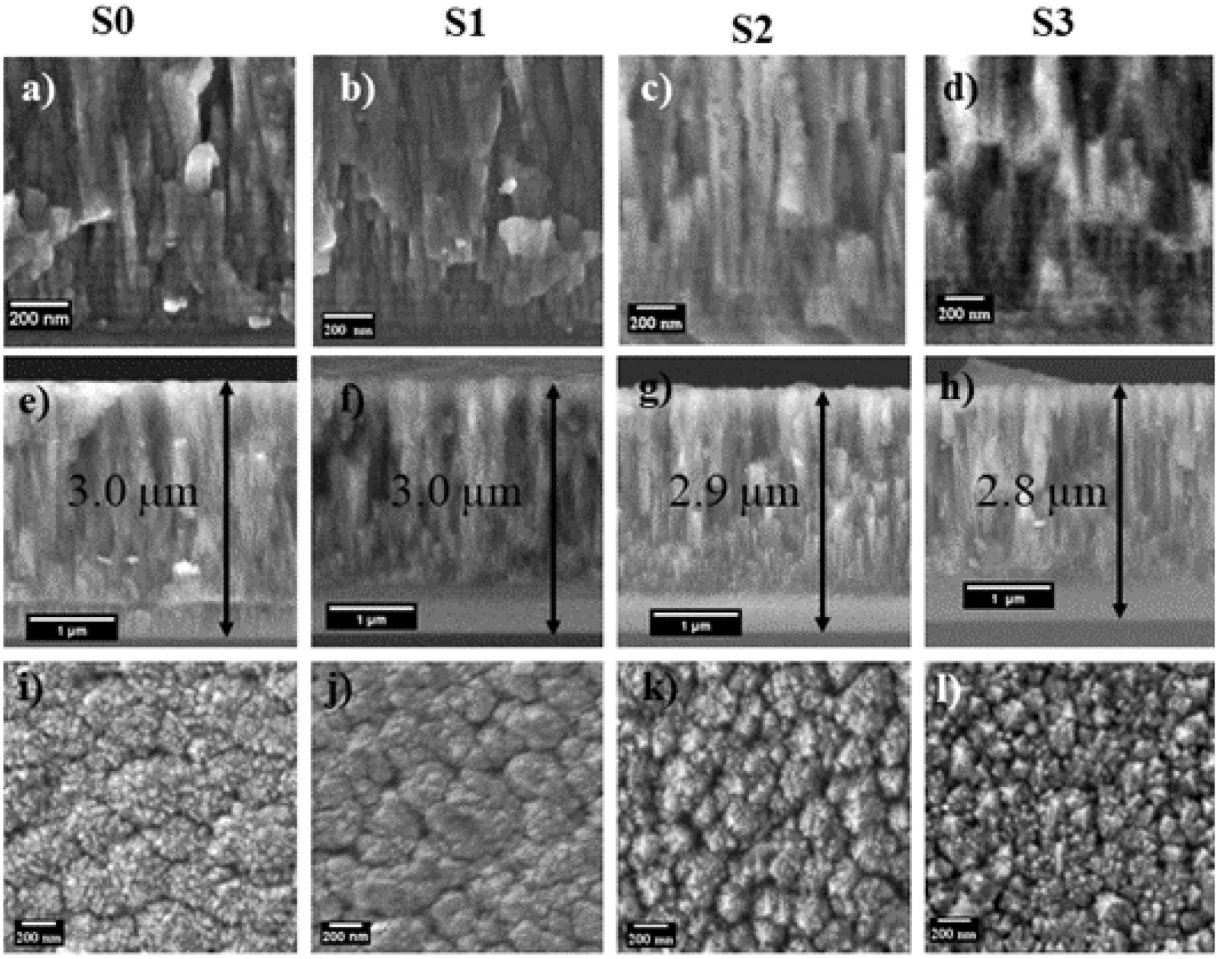

Fig. 1. Cross section and surface morphology of multilayered coatings: a–d) high resolution cross section SEM images of S0 to S3 coatings showing the nano-multilayer structure with superlattice period of ~40 nm, e–h) low resolution cross section SEM images of S0 to S3 coatings showing the their thickness and i–l) top surface images of S0 to S3 coatings.

orientation. Ag alloying increases the intensity of the (111) diffraction peak, suggesting the formation of a more pronounced (111) texture. Ag incorporation to films progressively decreases the level of residual compressive stresses, as presented in Table 1. However, no shift of the XRD diffraction peaks to higher diffraction angles were noticed. As the XRD diffraction peaks result on the superposition signals from the lattice parameters of the individual Ti(Ag)N and TiSiN layers in the multilayered structure, suggesting that a part of silver can be incorporated in the TiN lattice of the TiN(Ag) layer, counteracting the effect of the decrease of the compressive residual stresses. The decrease of residual stresses with Ag additions is likely due to the incorporation of Ag as a softer phase in the TiN structure which allows the residual stresses accommodation. This corroborates well with our previous [20] and other works, where the influence of Ag alloying on other coating systems was evaluated [28,39]. No Si-N crystalline phase was detected by XRD. For deposition performed at low mobility and/or bombarding conditions, as it is the present case, incorporation of Si in solid solution in the TiN matrix is expected [40]. Nevertheless, according to Houska et al. [41] the maximum Si content able to be incorporated into the TiN lattice is approximately 4 at.% and, above this threshold, the Si-N phase starts to form. Thus, despite of the global Si content in the multilayers films was in the range 4.3 to 4.8 at.%, in the single TiSiN layer it is much higher being expected that the presence of Si could be either in solid solution or as a Si-N phase. The absence of Si-N phase in the XRD diffractograms is correlated with its amorphous character as observed by different authors who have developed and studied Ti-Si-N films [16,20,23,33,42]. Ag diffraction peaks are also absent from the XRD diffractograms. Considering that in monolithic TiAgN coatings we could only detect Ag for contents ≥6.4 at.% (see vestiges of a peak positioned at ~38.1° at spectrum e) in Fig. 2)), the absence of Ag signal on the multilayered films is attributed to the presence of very small nanoparticles undetectable by XRD, as reported by Ju et al. [43], who conducted deep TEM studies on TiN-Ag films.

3.3. Adhesion critical loads, mechanical properties and thermal stability

The substrate-film adhesion of the coatings is essential for testing their mechanical properties and thermal stability, especially at high temperatures. All coatings showed a very good adhesion to the substrate (Fig. 3). No type of failure was detected for TiSiN/TiN reference film; however, when Ag was added, a failure by coating chipping - Lc2, could be detected. Globally, a small decrease of Lc2 load was observed with increasing Ag content. This behavior can be attributed to the decrease of the toughness of the films with silver addition, as suggested by the decrease in elastic strain to failure parameter, as shown in Table 1.

Hardness and elastic modulus of the as deposited and annealed at 800 °C coatings are shown in Fig. 4. As expected, the as deposited reference sample S0 shows the highest hardness (26 GPa) and elastic Young's modulus (334 GPa) among all the coatings. These values are similar to those of the work of Wo et al. [44,45] who deposited TiN/TiSiN multilayered coatings with similar period thickness. Xu et al. [7] and Cao et al. [8] achieved harder TiN/TiSiN multilayered coatings, in the range of 40 GPa, but their coatings superlattice period was lower,

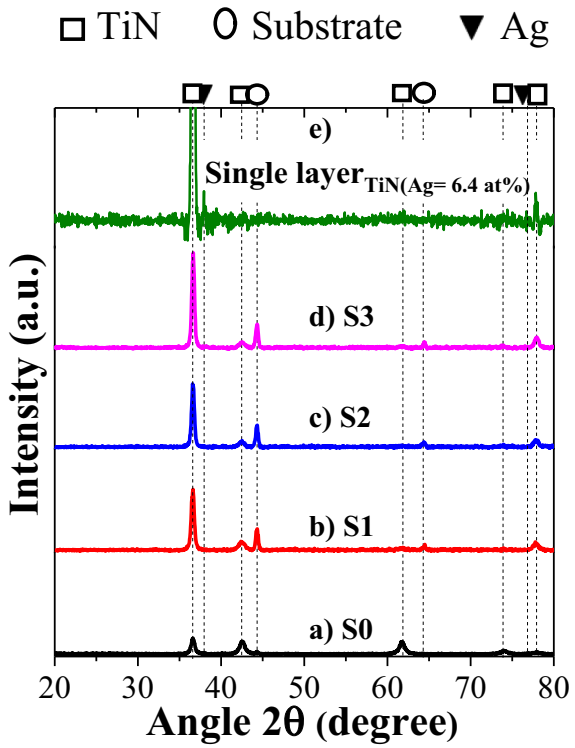

Fig. 2. XRD diffraction patterns of the coatings obtained in the conventional mode.

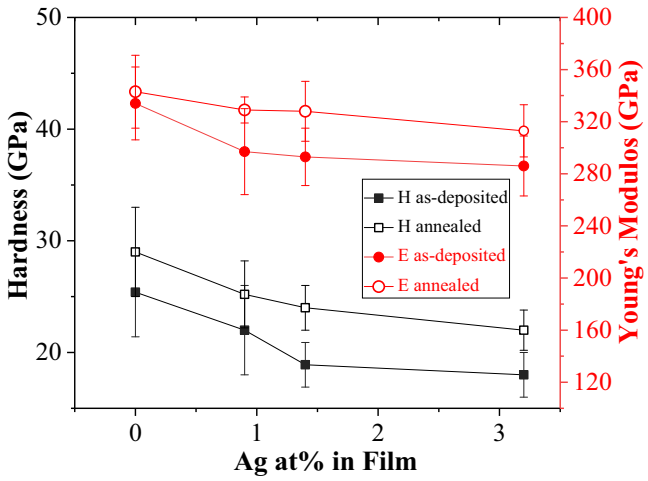

Fig. 4. Hardness and Young's modulus of coatings in as-deposited and annealed conditions. Annealing was conducted at 800 °C for 2 h.

10.3 nm and 12 nm, respectively. Ag doping, progressively decreases the H and E values of multilayered films. This is an expected result, due to the inclusion of a softer and less stiff phase in the coatings, and it is in accordance with our previous work on the effect of Ag additions on the nanocomposite structure of Ti-Si-N films [20]. Other works also showed similar trends for the addition of Ag when alloying different coatings systems [28,42,46]. Annealing treatment globally increases the H and E values of the coatings, which can be attributed to the increase of films crystallinity, as shown by the XRD diffraction patterns obtained in conventional mode (Fig. 5), where no major changes were observed, with the exception of an increment of the peaks intensities. In spite of the annealing, no Ag diffraction peaks could be detected, result that, again, is attributed to the small amount of Ag in the coatings. Elemental line profiles acquired through the cross section, as well as chemical analysis on the surface of the annealed films, did not allow detecting any preferential accumulation of Ag close to the surface (see Fig. 6), suggesting that out-diffusion of this element is not occurring. The concentration of the other chemical elements also remained constant across the thickness of the films. Therefore, in vacuum conditions this multilayer structure offers an efficient control of Ag, which can be a lubricious element, diffusion to the surface. It should be highlighted that similar annealing treatment applied to TiSiAgN coatings deposited with a nanocomposite structure in our previous work [20], also did not promote any change on the elements distribution in cross section. However, the EDS elemental mapping after protective annealing recorded the diffusion of Ag from a region close to the top was observed, leaving behind a very thin Ag depleted layer. Multilayer structure seems, thus, to offer a better barrier to Ag diffusion than nanocomposite structure.

3.4. Continuous and isothermal oxidation in air

Thermo-gravimetric analysis (TGA) tests were performed to S0 and S3 films to evaluate the influence of Ag additions on either the onset point of oxidation or the isothermal oxidation resistance. The onset point of oxidation of selected coatings was evaluated by heating the coatings up to 1200 °C in air, at a constant temperature ramp of 20 °C/min and then cooled down to room temperature, whilst their

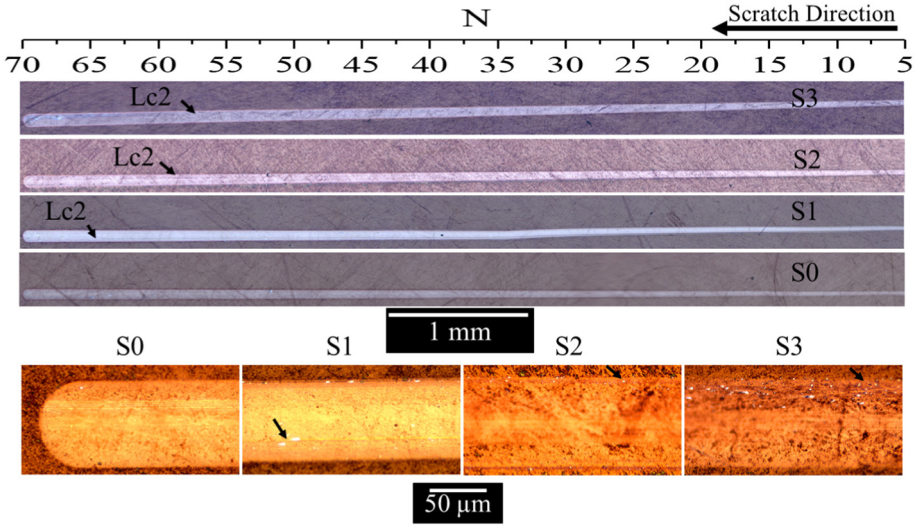

Fig. 3. optical microscope images of the scratch tests carried out for coatings deposited on tungsten carbide substrates, in the load range of 5–70 N.

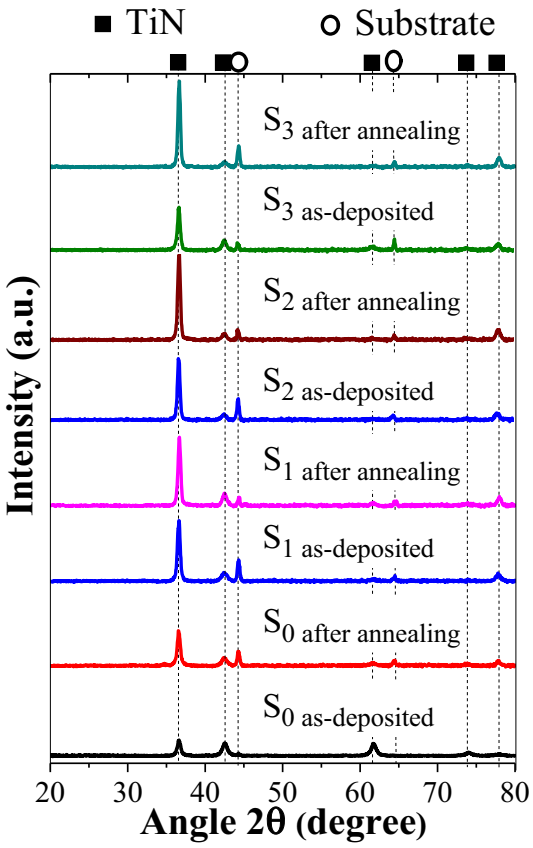

Fig. 5. XRD diffraction patterns of the coatings in as-deposited and after annealing at 800 °C for 2 h, obtained in conventional mode.

isothermal behavior was evaluated at 800 °C for 2 h (Fig. 7). The onset point of oxidation of reference film is around ~700 °C. Ag alloying does not change the onset point of oxidation. This corroborates our previous work where the addition of Ag to the nanocomposite TiSiN films did not affect the starting point of oxidation. However, this point is lower, by 150 °C, than the monolayer nanocomposite films studied in our previous work [33]. The low onset oxidation point of current coatings is primarily due to the presence of the TiN(Ag) layers in the multilayer arrangement which have much lower oxidation resistance (reported to be ~500 °C [47]) than any TiSiN film. The oxidation starting from the top surface and going down will take place layer by layer with a high rate in the Ti-N(Ag) layer and a lower rate in the Ti-Si-N layer. In the latter, the formation of Si-O or a mixture of Ti-Si-O protective oxide layers is responsible for ruling the oxidation performance of TiSiN films [48,49]. However, the very low thickness of this layer (in the order of 20 nm) makes difficult the formation of the continuous and protective oxide scales. Therefore, the barrier to the species participating in the oxidation process (either Ti^{4+}, Si^{4+}, Ag^{2+} or O^{2-} ions) is much less effective than in the thicker monolithic TiSiN with the consequent lower onset point of oxidation. Above the onset point temperature, the oxidation mass gain increases slowly in the temperature range of 750–900 °C. A sudden mass increase is then observed above this temperature up to the complete oxidation of the films occurring at ~1120 °C.

Isothermal oxidation tests were carried at 800 °C for both coatings, as seen in insert of Fig. 7. Both samples obey to a parabolic law of oxidation. However, Ag rich coating displayed a much higher parabolic rate constant than the TiSiN/TiN reference film.

The grazing XRD diffractograms of oxidized films are displayed in Fig. 8. TiSiN/TiN film shows diffraction peaks assigned to rutile TiO_2 and TiN crystallites revealing that the film was not totally oxidized. Diffraction peaks from the Al_2O_3 substrate could also be detected. No

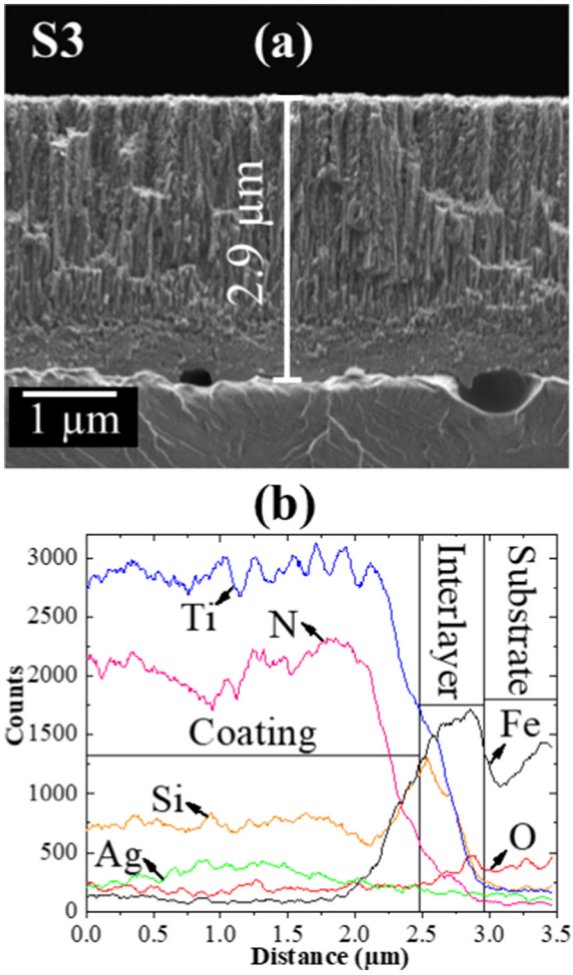

Fig. 6. a) Cross-section SEM image of annealed S3 coating and b) its corresponding EDS line depth profiles.

crystalline silicon-containing oxides were detected by XRD, suggesting their amorphous character as reported by different authors who also studied Si-containing coatings [47,50]. The cross-section morphology

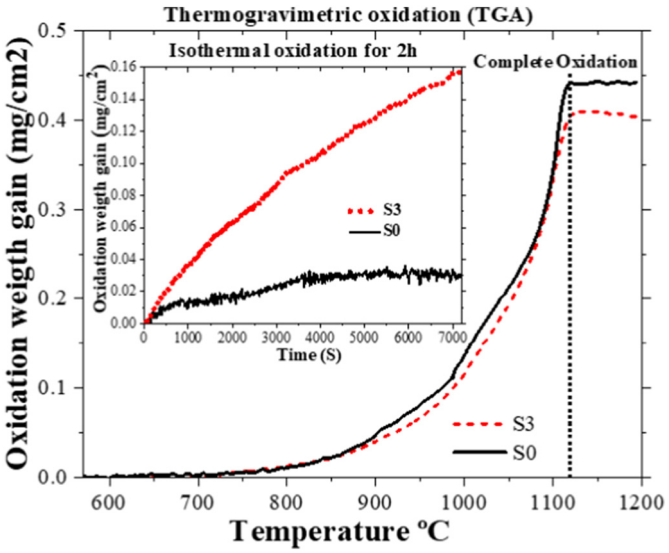

Fig. 7. Thermogravimetric oxidation rate of S0 and S3 performed at a constant linear temperature ramp (from RT to 1200 °C at a rate of 20 °C/min) and, in the inset, the isothermal TG curves of coatings exposed at 800 °C for 2 h.

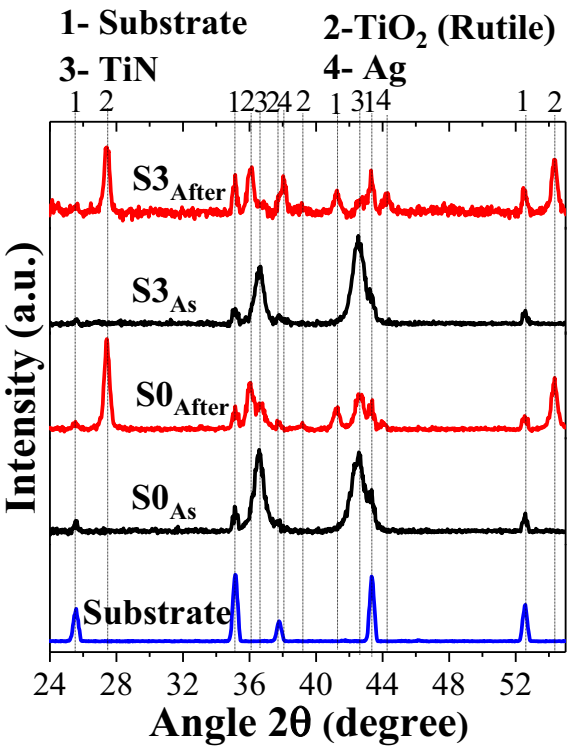

Fig. 8. XRD diffraction patterns acquired in grazing incidence mode for oxidized S0 and S3 coatings at 800 °C for 2 h.

of the oxidized film shown in Fig. 9 reveals the presence of an oxide scale with a total thickness of ~1.1 μm. According to the elemental lines analysis two zones can be distinguished: i) a very thin layer of TiO_2, corresponding to the sharp features on the top surface, and ii) a continuous and compact layer below, composed by Ti-Si-O, suggesting a mixture of Si and/or Ti oxides. This result is in line with the global oxidation of monolithic TiSiN films deposited as either solid solution or nanocomposite structures, for which the oxidation starts with a Ti-O layer growth on the top of the sample, followed by a Si-O or a mixture Ti-Si-O protective layers depending on the Si content in the films [47,50].

Concerning the XRD diffraction of oxidized S3 coating, similar phases as those indexed for the reference S0 film could be detected. In addition, peaks assigned to Ag could be detected. The Ag detection is in accordance with the analysis performed at the oxidized surface of the film, where agglomerates of silver (round features), could be observed, as shown in insert of Fig. 9b. Cross section morphology and EDS line profiles taken across the coating thickness (Fig. 10) revealed the formation of a dual oxide layer, as for the reference S0 film. However, bigger crystals of TiO_2 on the surface suggests a stronger Ti diffusion to the surface, as also shown by the thicker oxide scale, confirming the lower oxidation performance of the coating in the isothermal curve. The elemental maps confirm the accumulation of Ag in the top of the oxide scale as well as a thin layer, underneath, depleted of this element. This layer makes the interface with the remaining non-oxidized film and is attributed to the Ti-Si-O oxide. As its thickness is higher than the period of the as-deposited films, this means that silver diffuses from the remaining non-oxidized film to the interface with the oxide scale. Similar layer was observed by the authors for TiSiNAg films deposited with a nanocomposite structure [33]. Similarly, to the TiSiN/TiN reference film, Ti-

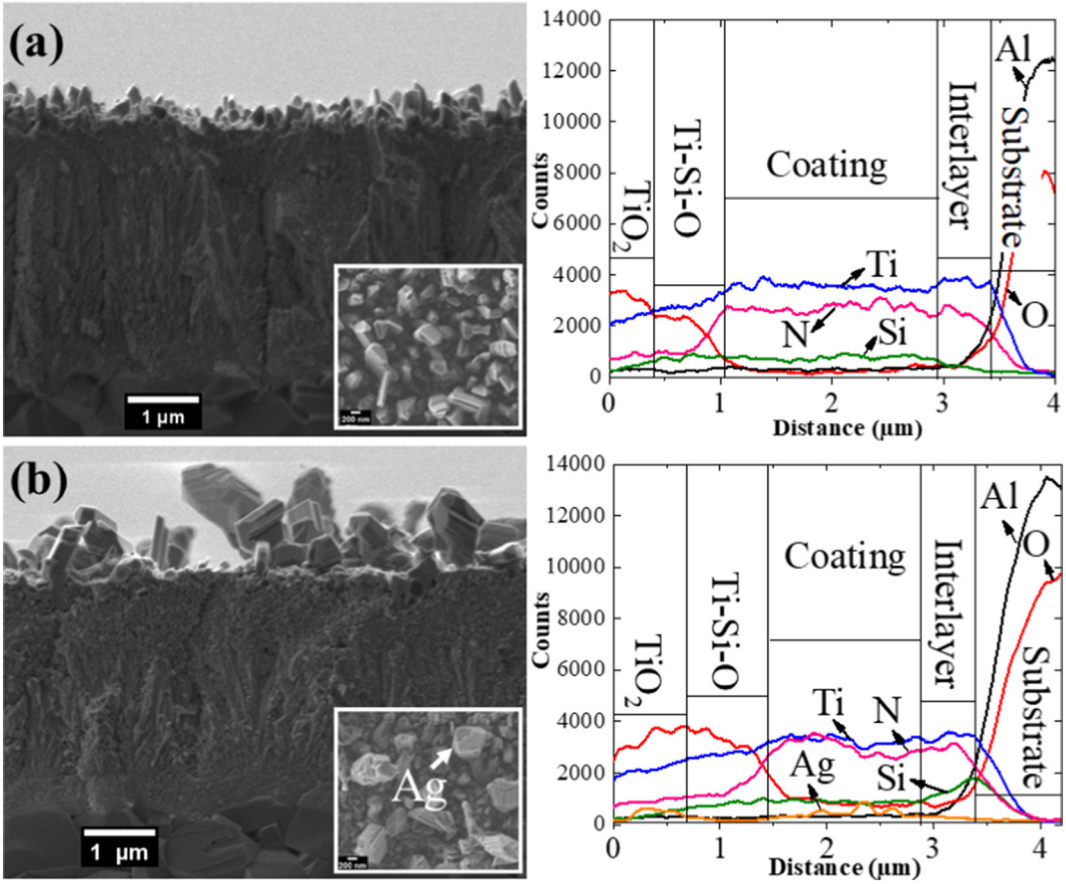

Fig. 9. Cross section morphology (left-hand side) with corresponding and elemental EDS line profiles (right-hand side) of: a) S0 and b) S3 films.

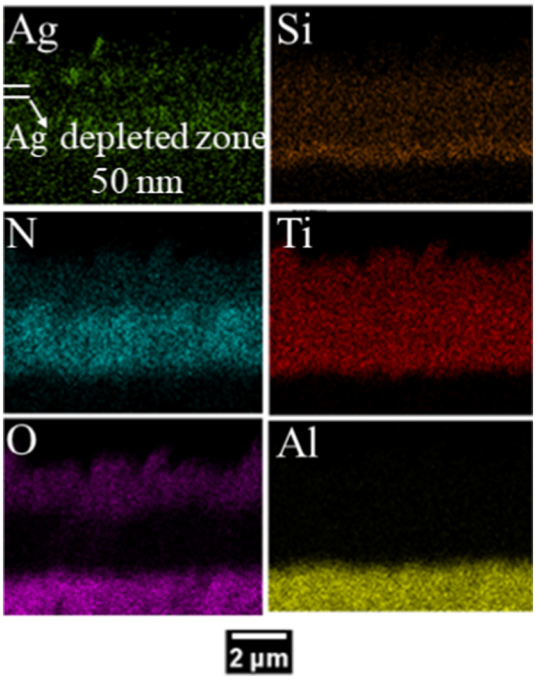

Fig. 10. Cross section EDS elemental maps distribution of the S3 coating after oxidation at 800 °C for 2 h.

O is formed firstly due to either the higher affinity of Ti than Si for oxygen or the much higher content of Ti than Si on the films, leaving behind a Ti-Si-O layer. However, due to the additional outwards diffusion of Ag, additional paths for ions diffusion will be created, i.e. Ag will interfere with the formation of a compact and protective Ti-Si-O layer, allowing higher fluxes of the species intervening in the oxidation process. Then, higher parabolic oxidation rates were measured for the Ag-containing coating.

Despite of the lower oxidation resistance of S3 coating, it should be highlighted that in the non-oxidized part of the film a constant signal of Ag is displayed; the Ag diffusion to the top, forming the agglomerates shown in Fig. 9b, simply results from the progressive oxidation of Ti and Si, leaving Ag unbonded and then, is free to move. Constant signal of Ag in the remaining film suggests that TiSiN layer in the multilayer structure offers an efficient control of the release of the lubricious phase, being a potential coating solution to provide long term lubrication, having practical interest in the industry. Transmission electron microscope (TEM) studies of the developed coatings are planned in the future to achieve further insight into coatings (micro)structure as well as on the importance of annealing treatments in the interfaces between the layers.

4. Conclusions

The present work reports on the influence of Ag additions on the morphology, structure, mechanical properties, thermal stability and oxidation resistance of multilayered TiSiN/Ti(Ag)N films deposited with low Ag contents (from 0 to 3.2 at.%). The results showed that all Ag rich films are over-stoichiometric as a result of the progressive poisoning of the target caused by the replacement of Ti by Ag pellets at the Ti target. As a consequence, a decrease of the deposition rate was also observed, despite of the higher sputtering rate of Ag as compared to the one expected from the Ti pellets. All coatings exhibit a face-centered cubic structure with a (111) preferred orientation; Ag alloying gives rise to a more pronounced (111) texture. All coatings were well adhered to the substrate; only one type of failure on the Ag rich coatings, Lc2 – first coating chipping, was possible to be identified, occurring for lower Lc2 values with increasing Ag addition. Hardness and Young's modulus of the films decreased with increasing Ag content due to the incorporation of softer Ag on the structure. Annealing treatment at protective atmosphere promoted an increase of the hardness and Young's modulus of the films. No diffusion of silver or change on the elements' distribution across the film thickness were observed which reveals a good thermal stability of the films. Ag alloying does not affect the start point of oxidation of films; however, oxidation resistance of Ag-containing films is lower as shown by isothermal oxidation tests carried out at 800 °C. SEM, together with XRD analysis, showed the formation of a dual oxide scale: on top rutile crystals and below a Ti-Si-O layer. The size of rutile crystals and the thickness of the inner Ti-Si-O layer increase with Ag incorporation due to the easier ions diffusion promoted by the additional Ag diffusion.

CRediT authorship contribution statement

A. AL-Rjoub: Conceptualization, Investigation, Methodology, Validation, Writing - original draft. **A. Cavaleiro:** Supervision, Project administration, Conceptualization, Writing - review & editing. **F. Fernandes:** Supervision, Conceptualization, Investigation, Validation, Writing - review & editing, Resources, Project administration, Funding acquisition.

Acknowledgements

This research is sponsored by FEDER Funds through Portugal 2020 (PT2020), by the Competitiveness and Internationalization Operational Program (COMPETE 2020) and national founds through the Portuguese Foundation for Science and Technology (FCT), under the projects: SMARTLUB - ref. "POCI-01-0145-FEDER-031807", CONTROLLUB - UT Austin Portugal Program ref. "UTAP-EXPL/NTec/0107/2017" and bilateral collaborative project between Portugal and India (Project number "441.00 INDIA"). This work is also supported by project CZ.02.2.69/0.0/0.0/18_070/0010457 in Czech Republic.

Declaration of competing interest

The authors declare that they have no known competing financial interests or personal relationships that could have appeared to influence the work reported in this paper.

Appendix A. Supplementary data

Supplementary data to this article can be found online at https://doi.org/10.1016/j.matdes.2020.108703.

References

[1] H. Randhawa, TiN-coated high-speed steel cutting tools, J. Vac. Sci. Technol. A 4 (2755) (2014) 4–8, https://doi.org/10.1116/1.573674.
[2] L. Wang, D.O. Northwood, X. Nie, J. Housden, A. Leyland, A. Matthews, Corrosion properties and contact resistance of TiN, TiAlN and CrN coatings in simulated proton exchange membrane fuel cell environments, J. Power Sources J. 195 (2010) 3814–3821, https://doi.org/10.1016/j.jpowsour.2009.12.127.
[3] M. Nose, Y. Deguchi, T. Mae, E. Honbo, T. Nagae, K. Nogi, Influence of sputtering conditions on the structure and properties of Ti – Si – N thin films prepared by RF -reactive sputtering, Surf. Coat. Technol. 174–175 (2003) 261–265, https://doi.org/10.1016/S0257-8972.
[4] T. Li, J. Xiong, Z. Guo, T. Yang, M. Yang, H. Du, Structures and properties of TiAlCrN coatings deposited on Ti(C,N)-based cermets with various WC contents, Int. J. Refract. Met. Hard Mater. 69 (2017) 247–253, https://doi.org/10.1016/j.ijrmhm.2017.08.020.
[5] L. Zhu, C. Song, W. Ni, Y. Liu, Effect of 10% Si addition on cathodic arc evaporated TiAlSiN coatings, Trans. Nonferrous Met. Soc. China. 26 (2016) 1638–1646, https://doi.org/10.1016/S1003-6326(16)64273-5.
[6] A.V. Pshyk, L.E. Coy, G. Nowaczyk, M. Kempiński, B. Peplińska, A.D. Pogrebnjak, V.M. Beresnev, S. Jurga, High temperature behavior of functional TiAlBSiN nanocomposite coatings, Surf. Coat. Technol. 305 (2016) 49–61, https://doi.org/10.1016/j.surfcoat.2016.07.075.
[7] Y.X. Xu, L. Chen, Z.Q. Liu, F. Pei, Y. Du, Improving thermal stability of TiSiN nanocomposite coatings by multilayered epitaxial growth, Surf. Coat. Technol. 321 (2017) 180–185, https://doi.org/10.1016/j.surfcoat.2017.04.057.

[8] J. Cao, K. Choy, H. Sun, H.-Q. Li, D. Teer, M.-D. Bao, Syntheses of nano-multilayered TiN/TiSiN and CrN/CrSiN hard coatings, J. Coat. Technol. Res. 8 (2) (2011) 283–288, https://doi.org/10.1007/s11998-010-9275-0.

[9] M.K. Samani, X.Z. Ding, N. Khosravian, B. Amin-ahmadi, Y. Yi, G. Chen, E.C. Neyts, A. Bogaerts, B.K. Tay, Thermal conductivity of titanium nitride/titanium aluminum nitride multilayer coatings deposited by lateral rotating cathode arc, Thin Solid Films 578 (2015) 133–138, https://doi.org/10.1016/j.tsf.2015.02.032.

[10] C. Chang, W. Chen, P. Tsai, W. Ho, D. Wang, Characteristics and performance of TiSiN/TiAlN multilayers coating synthesized by cathodic arc plasma evaporation, Surf. Coat. Technol. 202 (2007) 987–992, https://doi.org/10.1016/j.surfcoat.2007.06.024.

[11] P. Choi, I. Povstugar, J. Ahn, A. Kostka, D. Raabe, Thermal stability of TiAlN/CrN multilayer coatings studied by atom probe tomography, Ultramicroscopy 111 (2011) 518–523, https://doi.org/10.1016/j.ultramic.2010.11.012.

[12] Y.Y. Wang, M.S. Wong, W.J. Chia, J. Rechner, W.D. Sproul, Synthesis and characterization of highly textured polycrystalline AlN/TiN superlattice coatings, J. Vac. Sci. Technol. A 16 (1998) 3341, https://doi.org/10.1116/1.581542.

[13] C.M. Koller, R. Hollerweger, C. Sabitzer, R. Rachbauer, S. Kolozsvári, J. Paulitsch, P.H. Mayrhofer, Thermal stability and oxidation resistance of arc evaporated TiAlN, TaAlN, TiAlTaN, and TiAlN/TaAlN coatings, Surf. Coat. Technol. 259 (2014) 599–607, https://doi.org/10.1016/j.surfcoat.2014.10.024.

[14] V.P. Tabakov, A.S. Vereschaka, A.A. Vereschaka, Multilayer composition coatings for cutting tools: formation and performance properties, Mech. Ind. 18 (2017) 706, https://doi.org/10.1051/meca/2017063.

[15] I. Shyha, S.L. Soo, D.K. Aspinwall, S. Bradley, S. Dawson, C.J. Pretorius, Drilling of Titanium/CFRP/Aluminium stacks, Key Eng. Mater. 447–448 (2010) 624–633, https://doi.org/10.4028/www.scientific.net/KEM.447-448.624.

[16] J.C. Oliveira, F. Fernandes, F. Ferreira, A. Cavaleiro, Tailoring the nanostructure of Ti – Si – N thin fi lms by HiPIMS in deep oscillation magnetron sputtering (DOMS) mode, Surf. Coat. Technol. 264 (2015) 140–149, https://doi.org/10.1016/j.surfcoat.2014.12.065.

[17] N. He, H. Li, L. Ji, X. Liu, H. Zhou, J. Chen, High temperature tribological properties of TiAlSiN coatings produced by hybrid PVD technology, Tribol. Int. J. 98 (2016) 133–143, https://doi.org/10.1016/j.triboint.2016.02.034.

[18] T.D. Nguyen, S.K. Kim, D.B. Lee, High-temperature oxidation of nano-multilayered TiAlCrSiN thin films in air, Surf. Coatings Technol. 204 (2009) 697–704, https://doi.org/10.1016/j.surfcoat.2009.09.008.

[19] A.V. Bondarev, D.G. Kvashnin, I.V. Shchetinin, D.V. Shtansky, Temperature-dependent structural transformation and friction behavior of nanocomposite VCN-(Ag) coatings, Mater. Des. 160 (2018) 964–973, https://doi.org/10.1016/j.matdes.2018.10.029.

[20] D. Cavaleiro, S. Carvalho, A. Cavaleiro, F. Fernandes, TiSiN(Ag) films deposited by HiPIMS working in DOMS mode: effect of Ag content on structure, mechanical properties and thermal stability, Appl. Surf. Sci. 478 (2019) 426–434, https://doi.org/10.1016/j.apsusc.2019.01.174.

[21] T.L. Brzezinka, J. Rao, M. Chowdhury, J. Kohlscheen, G.S.F. Rabinovich, S.C.V. Id, J.L. Endrino, Hybrid Ti-MoS2 coatings for dry machining of Aluminium alloys, Coatings. 7 (149) (2017) 1–13, https://doi.org/10.3390/coatings7090149.

[22] K. Kutschej, P.H. Mayrhofer, M. Kathrein, P. Polcik, C. Mitterer, Influence of oxide phase formation on the tribological behaviour of Ti – Al – V – N coatings, Surf. Coat. Technol. 200 (2005) 1731–1737, https://doi.org/10.1016/j.surfcoat.2005.08.044.

[23] F. Fernandes, J.C. Oliveira, A. Cavaleiro, Self-lubricating TiSi(V)N thin films deposited by deep oscillation magnetron sputtering (DOMS), Surf. Coat. Technol. 308 (2016) 256–263, https://doi.org/10.1016/j.surfcoat.2016.07.039.

[24] A. Vladescu, V. Braic, M. Braic, M. Balaceanu, Arc plasma deposition of TiSiN/Ni nanoscale multilayered coatings, Mater. Chem. Phys. 138 (2013) 500–506, https://doi.org/10.1016/j.matchemphys.2012.12.010.

[25] C. Cancellieri, E. Klyatskina, M. Chiodi, J. Janczak-rusch, L.P.H. Jeurgens, The effect of interfacial Ge and RF-bias on the microstructure and stress evolution upon annealing, Appl. Sci. 8 (2403) (2018) 1–13, https://doi.org/10.3390/app8122403.

[26] F. Moszner, C. Cancellieri, M. Chiodi, S. Yoon, D. Ariosa, J. Janczak-rusch, Thermal stability of cu/W nano-multilayers, Acta Mater. 107 (2016) 345–353, https://doi.org/10.1016/j.actamat.2016.02.003.

[27] S. Li, J. Deng, G. Yan, K. Zhang, G. Zhang, Microstructure, mechanical properties and tribological performance of TiSiN–WS2 hard-lubricant coatings, Appl. Surf. Sci. 309 (2014) 209–217, https://doi.org/10.1016/j.apsusc.2014.05.012.

[28] C. Dang, J. Li, Y. Wang, Y. Yang, Y. Wang, J. Chen, Influence of multi-interfacial structure on mechanical and tribological properties of TiSiN/Ag multilayer coatings, J. Mater. Sci. 52 (2017) 2511–2523, https://doi.org/10.1007/s10853-016-0545-9.

[29] Z. Zhou, W.M. Rainforth, D.B. Lewis, S. Creasy, J.J. Forsyth, F. Clegg, A.P. Ehiasarian, P.E. Hovespian, W.-D. Munz, Oxidation behaviour of nanoscale TiAlNy/VN multilayer coatings, Surf. Coat. Technol. 178 (2004) 198–203, https://doi.org/10.1016/j.surfcoat.2003.09.031.

[30] A.A. Voevodin, C. Muratore, S.M. Aouadi, Hard coatings with high temperature adaptive lubrication and contact thermal management: review, Surf. Coat. Technol. 257 (2014) 247–265, https://doi.org/10.1016/j.surfcoat.2014.04.046.

[31] D.S. Stone, S. Harbin, H. Mohseni, J. Mogonye, T.W. Scharf, C. Muratore, A.A. Voevodin, A. Martini, S.M. Aouadi, Technology lubricious silver tantalate fi lms for extreme temperature applications, Surf. Coat. Technol. 217 (2013) 140–146, https://doi.org/10.1016/j.surfcoat.2012.12.004.

[32] S.M. Aouadi, H. Gao, A. Martini, T.W. Scharf, C. Muratore, Lubricious oxide coatings for extreme temperature applications: a review, Surf. Coat. Technol. 257 (2014) 266–277, https://doi.org/10.1016/j.surfcoat.2014.05.064.

[33] D. Cavaleiro, A. Cavaleiro, S. Carvalho, F. Fernandes, Oxidation behaviour of TiSiN (Ag) films deposited by high power impulse magnetron sputtering, Thin Solid Films (2019), 137423. https://doi.org/10.1016/j.tsf.2019.137423.

[34] A. Inspektor, P.A. Salvador, Architecture of PVD coatings for metalcutting applications: a review, Surf. Coatings Technol. 257 (2014) 138–153, https://doi.org/10.1016/j.surfcoat.2014.08.068.

[35] P. Rehák, D. Holec, M. Cerný, Interface-induced electronic structure toughening of nitride superlattices, Surf. Coat. Technol. 325 (2017) 410–416, https://doi.org/10.1016/j.surfcoat.2017.06.065.

[36] F. Fernandes, M. Danek, T. Polcar, A. Cavaleiro, Tribological and cutting performance of TiAlCrN films with different Cr contents deposited with multilayered structure, Tribol. Int. 119 (2018) 345–353, https://doi.org/10.1016/j.triboint.2017.11.008.

[37] F. Fernandes, A. Loureiro, T. Polcar, A. Cavaleiro, The effect of increasing V content on the structure, mechanical properties and oxidation resistance of Ti – Si–V–N films deposited by DC reactive magnetron sputtering, Appl. Surf. Sci. 289 (2014) 114–123, https://doi.org/10.1016/j.apsusc.2013.10.117.

[38] S. Zhang, F. Yan, Y. Yang, M. Yan, Y. Zhang, J. Guo, Effects of sputtering gas on microstructure and tribological properties of titanium nitride films, Appl. Surf. Sci. 488 (2019) 61–69, https://doi.org/10.1016/j.apsusc.2019.05.148.

[39] F. Fernandes, T.B. Yaqub, A. Cavaleiro, Influence of Ag additions on the structure, mechanical properties and oxidation behaviour of Cr-O coatings deposited by HiPIMS, Surf. Coat. Technol. 339 (2018) 167–180, https://doi.org/10.1016/j.surfcoat.2018.02.025.

[40] R.F. Zhang, S. Veprek, Crystalline-to-amorphous transition in Ti1−xSixN solid solution and the stability of fcc SiN studied by combined ab initio density functional theory and thermodynamic calculations, Phys. Rev. B 76 (2007), 174105. https://doi.org/10.1103/PhysRevB.76.174105.

[41] J. Houska, J.E. Klemberg-Sapieha, L. Martinu, Atomistic simulations of the characteristics of TiSiN nanocomposites of various compositions, Surf. Coat. Technol. 203 (2009) 3348–3355, https://doi.org/10.1016/j.surfcoat.2009.04.021.

[42] C. Dang, J. Li, Y. Wang, Y. Yang, Y. Wang, J. Chen, Influence of Ag contents on structure and tribological properties of TiSiN-Ag nanocomposite coatings on Ti– 6Al–4V, Appl. Surf. Sci. 394 (2017) 613–624, https://doi.org/10.1016/j.apsusc.2016.10.126.

[43] H. Ju, L. Yu, D. Yu, I. Asempah, J. Xu, Microstructure, mechanical and trobological properties of TiN-Ag films deposited by reactive magnetron sputtering, Vaccum 141 (2017) 82–88, https://doi.org/10.1016/j.vacuum.2017.03.026.

[44] P.C. Wo, P.R. Munroe, Z.F. Zhou, Z.H. Xie, K.Y. Li, Cross-sectional transmission electron microscopy of deformed microstructures in monolithic and multilayer TiSiN/TiN films, Int. J. Mod. Phys. B. 24 (2010) 18–25, https://doi.org/10.1142/S0217979210063934.

[45] W. Li, P. Liu, X. Zhu, K. Zhang, F. Ma, X. Liu, X. Chen, D. He, Influence of TiN-nanolayered insertions on microstructure and mechanical properties of TiSiN nanocomposite film, J. Mater. Sci. 49 (2014) 4127–4132, https://doi.org/10.1007/s10853-014-8107-5.

[46] C. Dang, M. Dong, J. Li, Influence of annealing temperature on film morphology and tribological performance of TiSiN-Ag coating, Mater. Res. Express. 6 (2019).

[47] Y. Yin, L. Hang, S. Zhang, X.L. Bui, Thermal oxidation properties of titanium nitride and titanium – aluminum nitride materials — a perspective for high temperature air-stable solar selective absorber applications, Thin Solid Films 515 (2007) 2829–2832, https://doi.org/10.1016/j.tsf.2006.03.042.

[48] M. Diserens, J. Patscheider, F. Le, Mechanical properties and oxidation resistance of nanocomposite TiN – SiNx physical-vapor-deposited thin films, Surf. Coat. Technol. 121 (1999) 158–165, https://doi.org/10.1016/S0257-8972(99)00481-8.

[49] D. Pilloud, J.F. Pierson, M.C.M. De Lucas, A. Cavaleiro, Study of the structural changes induced by air oxidation in Ti – Si – N hard coatings, Surf. Coat. Technol. 202 (2008) 2413–2417, https://doi.org/10.1016/j.surfcoat.2007.09.017.

[50] F. Deschaux-Beaume, T. Cutard, N. Fre, C. Levaillant, C. Jarlard, Oxidation of a silicon nitride – titanium nitride composite: microstructural investigations and phenomenological modeling, J. Am. Ceram. Soc. 85 (7) (2002) 1860–1866.